Numerical modeling of the hygro-mechanical behavior of the 3D composite materials

Mamadou Abdoul Mbacké, Shahram Khazaie, Sylvain Fréour, Frédéric Jacquemin

Numerical modeling of the hygro-mechanical behavior of the 3D composite materials

Journal Title
XX(X):1–15

DOI: 10.1177/ToBeAssigned
www.sagepub.com/
SAGE

Mamadou Abdoul Mbacké[1],Shahram Khazaie[2],Sylvain Fréour[2] and Frédéric Jacquemin[2]

Abstract

The composite materials used in marine environments are subjected to mechanical loads along with the water absorption. The analysis of the behavior of such materials requires to take into account the coupling between the mechanical and diffusion behaviors. The hygro-mechanical coupling has been widely investigated experimentally and numerically. This paper presents a numerical approach to model the hygro-mechanical coupling of composite materials. The diffusion process is modeled via the classical Fick's law. The elasticity matrix is considered to belong to transverse isotropic class, i.e. the composite studied is a unidirectional one. The components of the former are considered as moisture content dependent. The constitutive law takes into account on the one hand the strain induced by the hygroscopic swelling and on the other hand the dependence of the mechanical properties (elastic constants along with the material ultimate strengths) on the moisture content. These are implemented in a finite element software used to investigate the influence of the hygro-mechanical coupling on the composite material behavior. The robustness of our numerical tool is investigated with some numerical case studies.

Keywords

Hygro-mechanical coupling, Degradation of elastic properties, Composite materials

1 Introduction

Lightening of structures, particularly in the field of Marine Renewable Energy (MRE), is a growing research topic that aims at increasing technical, economical and environmental performances of the structures. In this regard, the composite materials have great potentials. Nevertheless, it is essential to take into account the water diffusion through the composite materials in order to better estimate their long-term behavior.

When a more or less porous material is exposed to a liquid medium, it absorbs water through its immersed surfaces, then the water spreads across its volume according to physical diffusion laws: it thus results in a mass uptake. During the last decades, numerous works have been devoted to the humid aging of the composite materials Peret et al. (2014); Rambert and Grandidier (2005). Several models such as Fick, two-stage Fick and Langmuir diffusion processes are among the diffusion models that are widely used in the literature Carter and Kibler (1978); Langmuir (1916). Fick's law is the most frequently used Crank (1979); Fick (1855) that enables to model the diffusion process for most polymers and composites. In this work, only the Fickian materials will be considered.

Beyond the diffusion phenomenon, it is necessary to assess the consequences of the diffusion on the mechanical performance of composites Weitsman (2000); Simar et al. (2014). The influence of the moisture on the mechanical behavior of composites is quite complex. According to the literature, many material properties are likely to be affected by the humid aging Bonniau and Bunsell (1981); Castaing and Lemoine (1995); Dewimille and Bunsell (1983); I. Ghorbel and Spiteri (1990); Shen and Springer (1976); Tual et al. (2015); Mei et al. (2019); Gager et al. (2019). Conversely, the moisture absorption rate and the maximum absorption capacity of composites could be affected by the mechanical loading Fahmy and Hurt (1980); Yaniv and Ishai (1987).

[1]Institut de Recherche Technologique (IRT) Jules Verne, Chemin du Chaffault, 44340 Bouguenais, France
[2]Université de Nantes - Centrale Nantes, Institut de Recherche en Génie Civil et Mécanique (UMR CNRS 6183), 58 Rue Michel Ange, BP 420, 44606 Saint-Nazaire, France

Corresponding author:
Mamadou Abdoul Mbacké.
Email: mamadou.mbacke@irt-jules-verne.fr

One of the main consequences of the water diffusion is the differential swelling which results in internal hygroscopic stresses Sar et al. (2014). However, for instance Derrien and Gilormini (2009) showed that the hygroscopic swelling cannot be freely developped in the case of composite materials where reinforcements do not absorb water. This results in internal stresses that prevent the polymer matrix from absorbing as much water as it would if it were free to swell. In addition, the experimental studies have demonstrated the influence of moisture on several mechanical properties. The results obtained by Tual et al. (2015) and Mercier et al. (2008) revealed a fall down of the shear and transverse Young moduli along with corresponding strengths as the moisture content increases in the composite. Aldajah et al. (2009) also observed a decrease in the flexural modulus of the composite materials as a function of the moisture content. Li et al. (2016) measured the propagation velocity of the Lamb waves through the laminated composite materials subjected to the water diffusion. They observed a decrease of the velocity which was linked to as possible degradation of the mechanical properties of the material. Ahmad et al. (2018) investigated the influence of humidity on the mechanical properties of hybrid hemp/polyethylene terephthalate (PET) composites following a dynamic mechanical analysis. Their result are also confirmed by Chouhan et al. (2019) through investigating the effect of moisture absorption on the compressive high strain rate performance of Ultra High Molecular Weight Polyethylene-Synthetic Rubber composite along the thickness direction. From the aforementioned experimental studies, it can be concluded that in the presence of humidity, the mechanical properties decrease.

Several numerical works have been carried out to model the diffusion and mechanical behaviors of the structures immersed in water. The simplest approach uses a hygro-elastic law in which case the water diffusion is only considered, yielding a hygroscopic strain Peret et al. (2014): modeling is based on the usage of the Hooke and Fick laws separately. In order to obtain more realistic predictions of the behavior of immersed polymer or composite materials, several studies have investigated the coupling (interaction) between diffusion and mechanics Mercier et al. (2008); Rambert and Grandidier (2005); B. E. Sar and Jacquemin (2012); Youssef et al. (2009a); Jacquemin and Fréour (2014). A state of the art on these works reveals two main approaches to model this coupling: approach based on thermodynamics of irreversible processes and approach based on the free volume theory.

The first approch is used for polymers to model the thermo-hygro-mechanical coupling in the context of explosive decompression Rambert and Grandidier (2005) along with the hygro-mechanical coupling in the context of water absorption B. E. Sar and Jacquemin (2012). The consistency of this thermodynamic approach has also been highlighted by other works. For instance the works of Roy (2000) for modelling non-Fickian diffusion in viscoelastic polymers and ploymer composite and those of Hassani et al. (2015) who proposed a 3D orthotropic elasto-plastic, visco-elastic, mechano-sorptive constitutive model for wood, with all material constants being defined as a function of moisture content. However, thermodynamic approaches generally involve many internal state variables that are sometimes difficult to characterize experimentally.

Approach that is based on the free volume theory Peret et al. (2014); Youssef et al. (2009a); Clément et al. (2018) is also used to model hygro-mechanical coupling. This approach is inspired by the studies performed on polymers Adamson (1980); E. L. McKague Jr. and Halkias (1978) where it is supposed that the fluid can only diffuse in a given volume of the structure called the free volume, i.e. neglecting water molecules - polymer interactions. The latter is the difference between the volume of the polymer and the volume actually occupied by the molecules that constitute it. An extension of this approach to fibre-reinforced polymer composites could probably be possible using multi-scale modelling, but would be difficult to apply to macroscopic modelling unless a scale transition method is used to determine the homogenized properties of the composite Youssef et al. (2009b). Apart from these two approaches, we can cite the works of Moleiro et al. (2019, 2020) based on the development of layerwise mixed model to describe the thermo-hygro-mechanical behavior of multilayer composite plates.

We propose a pragmatic and adapted approach to model the coupled hygro-mechanical behavior of the composite materials immersed in water. This approach is based on an evolution of structure's stiffness matrix and mechanical strengths according to the average moisture content and thus the immersion time. The particularity of our approach is related to the ease of obtaining the input material parameters compared to the thermodynamic approach being complicated since it has many parameters and to the approach based on the free volume theory which is difficult to be adapted to the structure's scale. In the case of a linear evolution of mechanical properties with respect to water content, only dry and saturated mechanical properties are required for the coupled model. For this purpose, we develop a Abaqus user

defined element (UEL) subroutine. One of the advantages of implementing Abaqus user defined element is the possibility to integrate degrees of freedom and couplings not taken into account by the classical finite elements available in the commercial code used. For example, various two- and three-dimensional Abaqus user defined element (UEL) subroutines are recently used for modeling the diffusion-deformation coupling of the elastomeric gels Chester and Anand (2011); Chester et al. (2015).

The outline of the paper is the following. In section 2, we introduce the studied material and the method used to model of the hygro-mechanical coupling problem for composite materials. A Fickian kinetics is used to model the sorption curve and the influence of the local water content on the components of the elasticity matrix is discussed. In the following section (3), a finite element framework is developed in order to be able to numerically implement the user element (UEL) subroutine. The latter is subsequently used in section 4 to verify the proper evolution of the components of the elasticity matrix and then the validation with classical Abaqus elements is carried out. Finally, we compared linear, bilinear and polynomial models. The conclusions and perspectives are given in Section 5.

2 Materials and modeling methods

2.1 Description of the material

The material under study is a carbon fiber reinforced vinyl ester matrix composite manufactured by infusion process. It is a unidirectional composite with a fiber volume fraction of about 46 %. A gravimetric study consisting in measuring the mass evolution of specimens immersed in water as a function of the ageing time is carried out to quantify the water diffusion kinetics of the vinylester resin. Five plates with dimensions of 100 mm×100 mm×3 mm are immersed for 10 months for this gravimetric study. It results from the water content – square root of the immersion time curve (see Figure 1) that the diffusion of water in the resin corresponds to a Fickian-type evolution and thus can be represented by Fick's law. Indeed, since carbon fibers are hydrophobic, we assume that the overall diffusion kinetics in the carbon fiber/vinylester composite is governed by that of the resin and therefore corresponds to a Fickian-type evolution Figliolini and Carlsson (2014).

The three dimensional Fick's law is used to model the diffusion process:

$$\frac{\partial c(\mathbf{x},t)}{\partial t} = D_x \frac{\partial^2 c}{\partial x^2} + D_y \frac{\partial^2 c}{\partial y^2} + D_z \frac{\partial^2 c}{\partial z^2} \quad (\mathbf{x},t) \in \Omega \times \mathbb{R}^+, \tag{1}$$

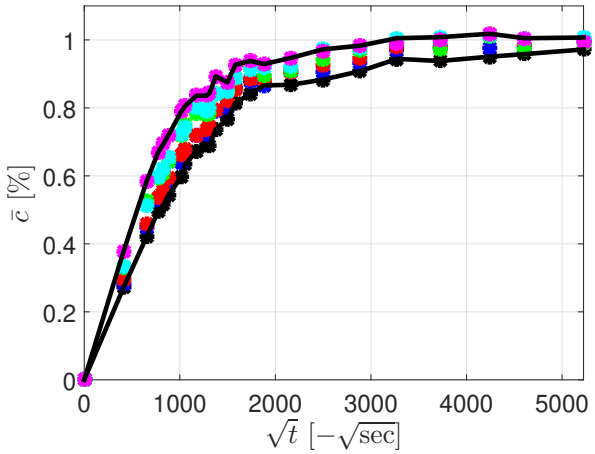

Figure 1. Experimental data showing a Fickian diffusion of the moisture content through the samples: each color represents the result of a given immersed plate.

in which c denotes the moisture content over the medium $\Omega = \mathbb{R}^3$ at each time t, and D_x, D_y and D_z specify the diffusion constants following each space direction. The latter are a priori functions of the mechanical state of the medium, i.e.

$$D_i(\mathbf{x},t) = \mathcal{F}_i(\boldsymbol{\sigma}(\mathbf{x},t)), \quad i \in \{x,y,z\}, \tag{2}$$

wherein $\boldsymbol{\sigma}(\mathbf{x},t)$ is the stress tensor at time t and at the point $\mathbf{x}$. It is worth noticing that the local moisture content cannot be easily measured experimentally. The experimental results usually allow the identification of a global diffusion coefficient. By contrast, obtaining the corresponding coefficient for each direction needs more complex approaches. The moisture diffusion coefficient of the unidirectional composite in the direction parallel to the fibers D_x was identical to that of the neat resin Dana et al. (2013). Thus, analytical formulas are often proposed to calculate the values of D_y and D_z Dana et al. (2013); Springer and Tsai (1967). The average over the volume of the material $\bar{c}(t)$ could be measured at each instant:

$$\bar{c}(t) = \frac{1}{V_\Omega} \int_\Omega c(\mathbf{x},t) d\mathbf{x} \tag{3}$$

in which V_Ω denotes the volume occupied by the material.

A linear elastic behavior considering the hygroscopic swelling induced by water diffusion models the mechanical state of the system:

$$\boldsymbol{\sigma}(\mathbf{x},t) = C\left(\varepsilon(\mathbf{x},t) - \varepsilon^h(\mathbf{x},t)\right) \tag{4}$$

with C the fourth-rank elasticity tensor, ε the total strain and ε^h the hygroscopic strain. This elasticity tensor at each position depends a priori on the local moisture content, i.e.:

$$C(\mathbf{x},t) = \mathcal{G}_i(c(\mathbf{x},t)), \quad i \in \{x,y,z\}, \tag{5}$$

The full hygro-mechanical coupling is done by taking into consideration simultaneously the equations (2) and (5).

The development of the numerical approach (section 2.2) is based on data from the literature Tual et al. (2015). Tables 1 and 2 summarize respectively the elastic properties and ultimate stresses of the dry and aged composite in different directions. Table 3 also shows the values of D_x, D_y and D_z.

Table 1. Experimental data taken from Tual et al. (2015).

Mechanical parameter $\mathcal{F}(C_{ij})$	Initial state $\mathcal{F}(C_{ij}^0)$	Final state $\mathcal{F}(C_{ij}^f)$
E_{11} MPa	140000	140000
E_{22} MPa	7000	7000
G_{12} MPa	3600	2400
ν_{12} [−]	0.32	0.32
ν_{23} [−]	0.40	0.40

Table 2. Experimental data taken from Tual et al. (2015).

Tensile strength	Initial state	Final state
X_r [MPa]	2250	1500
G_{12} [MPa]	3600	2400
Y_r [MPa]	47	22
S_r [MPa]	69	55

Table 3. Data taken from Tual et al. (2015)

Diffusion coefficient	Value
D_x [mm^2/s]	5.62×10^{-8}
D_y [mm^2/s]	1.54×10^{-7}
D_z [mm^2/s]	1.54×10^{-7}

2.2 Modeling methods

The proposed approach is based on a progressive degradation of the elastic moduli along with the strengths. A failure criterion is subsequently used. The former also evolves in terms of the water content since it depends on the ultimate strengths which vary during the diffusion process.

2.2.1 Approach based on degradation of elastic properties and material strengths It has been noticed that the mechanical properties change according to the moisture content of the composite materials of a structure in humid environment. These facts have been confirmed by several experimental tests. For instance, Tual et al. (2015) observed a stiffness drop of composites during aging. Figure 2 shows the evolution of the longitudinal Young's modulus E_{11}, transverse Young's modulus E_{22} and shear modulus G_{12} as a function of the immersion time. Considering the initial and final states (the first and the last points), the Young's moduli E_{11} and E_{22} remain almost unchanged but the shear modulus varies from 3600 MPa to 2400 MPa. The same observation was made for the strengths with much larger decreases compared to those of the Young and shear moduli (Figure 3).

In an industrial context, a pragmatic and easy-to-implement

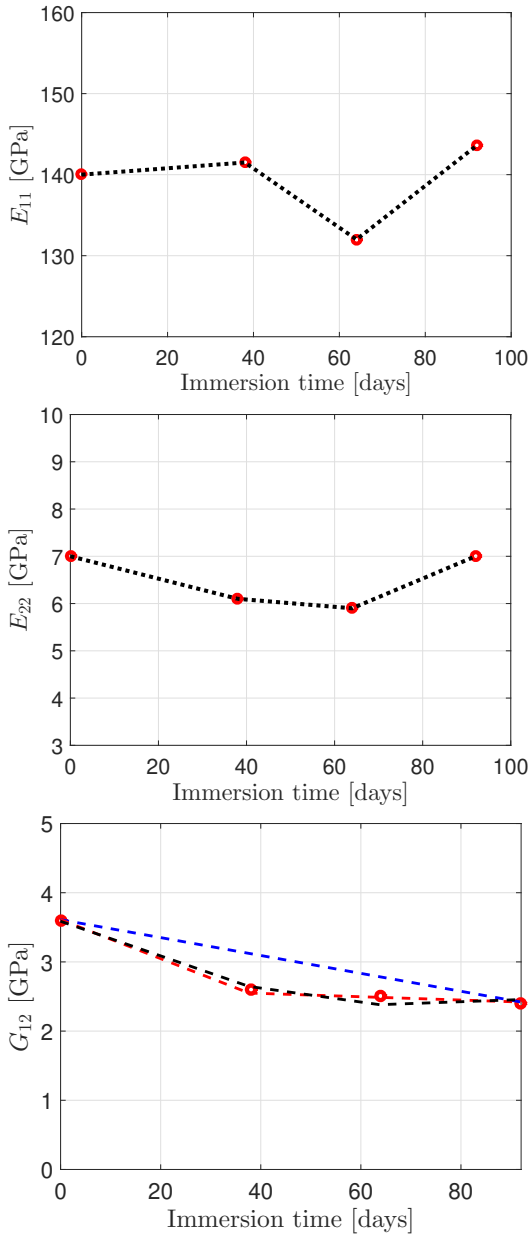

Figure 2. Evolution of mechanical properties as a function of immersion time: Longitudinal Young's Modules E_{11}(a), transverse Young's modulus E_{22}(b) and shear modulus G_{12}(c) Tual et al. (2015).

approach to model the mechanical-diffusion coupling is to take into account these gradual parameter (mechanical and/or diffusion) decrease in numerical simulations. This approach should in principle take into account two phenomena. On the one hand, moisture absorption lowers the mechanical properties and on the other hand the mechanical stresses have an effect on the diffusion law parameters. However, the latter is neglected in this study since no experimental data was at our disposal in order to take it in into account. Therefore, the hygro-mechanical coupling has been modeled by accounting

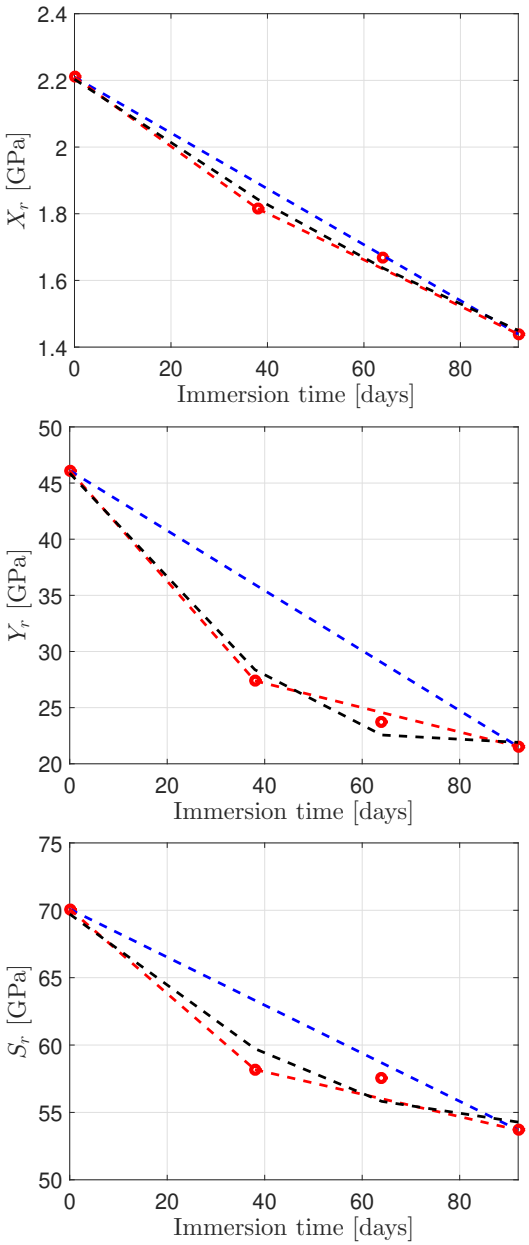

Figure 3. Evolution of longitudinal strength X_r(a), transverse strength Y_r(b) and shear strength S_r(c) as a function of immersion time (red points) Tual et al. (2015). The blue curves represent a linear approximation taking into account only the initial and final state values. The black curves are a third order polynomial approximation accounting for all four experimental data.

for a dependence of the coefficients of the stiffness matrix and strengths as a function of the moisture content.

With regard to the shape of the experimental curves (Figures 2 and 3), it turns out that a linear interpolation could be used to make an appropriate modeling. Thus, to model the decay of each coefficient of the stiffness matrix, one needs at least 2 tests. The advantage of a low-degree interpolation is that few experimental results are required to identify the model parameters. Especially in the case of first degree interpolation, only dry stiffness (zero moisture content) and aged one are required which are reasonable in an industrial context. In addition, the degree of interpolation can be enriched according to the available data. In this paper, a linear interpolation is mainly used and will be subsequently compared to the polynomial and bilinear approximations.

Hence, we propose to reduce these coefficients linearly in terms of the average moisture content on the medium $\bar{c}$, since the latter is the measurable quantity. We consider the first (dry state) and the last (aged state) points rather than doing a linear regression as it can be found in Figure 4 wherein the red dashed curve specifies the linear decrease of G_{12} during the immersion time. Knowing that the moisture content is directly related to the immersion time, we can express the values of G_{12} in terms of the (average) moisture content. In Figure 4, the blue line is a linear approximation which takes into account only the initial and final values of G_{12} and whose equation is $G_{12}(t) = -0.013t + 3.61$ in which G_{12} is in GPa and t is the immersion time in days. The red curve is a third order polynomial approximation whose equation is $G_{12}(t) = 0.000234t^2 - 0.033817t + 3.586975$.

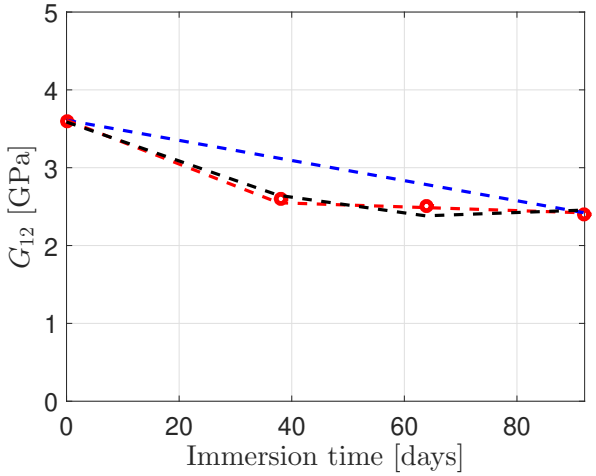

Figure 4. Variation of G_{12} in terms of the immersion time (red points). The blue curve represents a linear approximation taking into account only the initial and final state values. The black curve is a third order polynomial approximation accounting for all four experimental data.

The linear interpolation of the stiffness as a function of the average water content over each element $\bar{c}$ is thus considered. We propose to test a dry material and a test on an aged one. Our model then reads:

$$C(\bar{c}(t)) = C(c_0) + \left[\frac{C(c_\infty) - C(c_0)}{c_\infty}\right]\bar{c} \qquad (6)$$

in which c_∞ is the maximum moisture absorption capacity of the material, c_0 is the initial moisture content, $C(c_0)$ and $C(c_\infty)$ are the elasticity matrices at dry and aged states. Similarly for strengths, for instance for X_r, our linear

interpolation reads:

$$X_r(\bar{c}(t)) = X_r(c_0) + \left[\frac{X_r(c_\infty) - X_r(c_0)}{c_\infty}\right]\bar{c} \quad (7)$$

Using these formulas, the stress can be calculated at each aging level. The implementation algorithm can therefore be sequential: for each time step, the calculation of the local stiffness matrix is made from the local moisture content calculated with the Fick model (Eq. (1)). Then this matrix is used to carry out the mechanical calculation. Figure 5 depicts this algorithm. Moreover, the influence of the mechanical

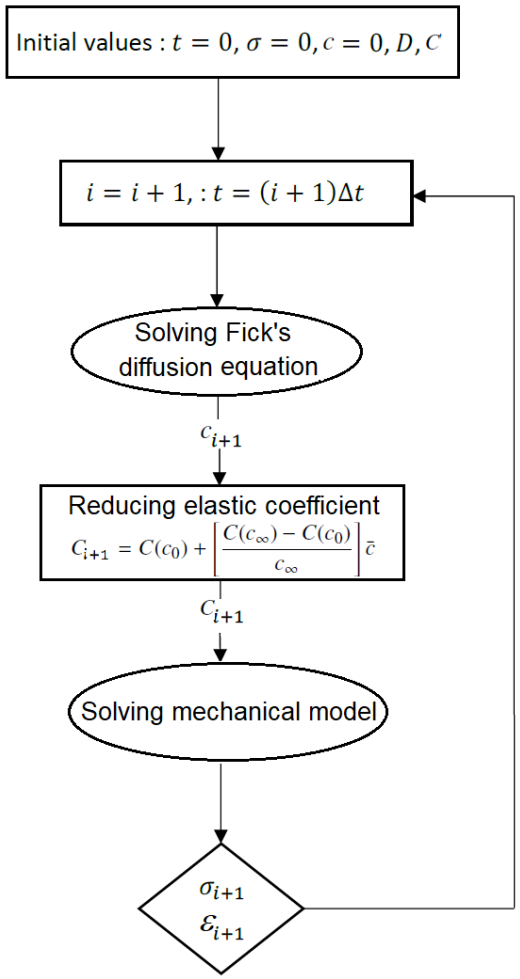

Figure 5. Algorithm of implementation of the evolution of the mechanical properties according to the diffusion state of the medium.

loading on the kinetics of water diffusion could not be taken into account due to the lack of experimental data. Thus, the diffusion coefficients are considered as constant throughout the mechanical loading.

2.2.2 Failure criteria The effects of hygrometry on the material properties and on the stresses, coupled with those of external mechanical loadings, can progressively generate damage which eventually cause the failure of the composite structure. Predicting the failure of composite structures is critical for their design. The purpose of the failure criteria is to predict the capability of a composite structure to withstand a certain type of loading and to enable the designer to evaluate its mechanical strength. In the corresponding literature, there are several failure criteria such as Tsaï-Wu Tsai and Wu (1971), Hashin Hashin (1980), Puck Puck (1969) and Tsaï-Hill Tsai (1965). We decided to implement the Tsaï-Hill criterion because it requires fewer parameters to be identified experimentally. In fact, the Tsaï-Hill criterion requires only the tensile failure strengths in three main directions x, y and z and three shear failure strengths: the particularity of the Tsaï-Hill criterion compared to the Tsaï-Wu is that it disregards the difference in behavior between traction and compression in x and y directions.

$$\begin{aligned}&\frac{1}{X_r^2(\bar{c})}\sigma_{11}^2 + \frac{1}{Y_r^2(\bar{c})}\sigma_{22}^2 + \frac{1}{Z_r^2(\bar{c})}\sigma_{33}^2 + \frac{1}{S_r^2(\bar{c})}\sigma_{12}^2 \\ &+ \frac{1}{R_r^2(\bar{c})}\sigma_{13}^2 + \frac{1}{Q_r^2(\bar{c})}\sigma_{23}^2 - \left(\frac{1}{X_r^2(\bar{c})} + \frac{1}{Y_r^2(\bar{c})}\right. \\ &\left. - \frac{1}{Z_r^2(\bar{c})}\right)\sigma_{11}\sigma_{22} - \left(\frac{1}{X_r^2(\bar{c})} - \frac{1}{Y_r^2(\bar{c})} + \frac{1}{Z_r^2(\bar{c})}\right)\sigma_{11}\sigma_{33} \\ &- \left(-\frac{1}{X_r^2(\bar{c})} + \frac{1}{Y_r^2(\bar{c})} + \frac{1}{Z_r^2(\bar{c})}\right)\sigma_{22}\sigma_{33} \quad (8)\end{aligned}$$

where (σ_{11}, σ_{22}, σ_{33}, σ_{12}, σ_{13}, σ_{23}) are the stresses obtained from the finite element simulation and the parameters of the criterion (X_r, Y_r, Z_r, S_r, R_r, Q_r) are respectively the failure stresses in x, y and z directions, the failure shear stresses in xy, xz and yz planes assuming a linear material behavior until a brittle failure. The particularity of the implemented criterion is that the strengths X_r, Y_r, Z_r, S_r, R_r and Q_r also evolve as a function of the moisture content. In the next section we elaborate the finite element formulation of the hygromechanical coupling using the approach introduced in Section 2 2.

3 Finite element formulation of the hygro-mechanical coupling

In this section, the stiffness matrix of the hygro-mechanical behavior with taking into account the degradation of mechanical parameters is derived. This stiffness matrix will be subsequently used in our User ELement (UEL) subroutine. The objective is thus to write the governing equations as the matrix (discretized) form $[\mathbf{K}]\{du\} = \{f\}$ in which $[\mathbf{K}]$ is the stiffness matrix. For this purpose, the weak formulation of the hygro-mechanical coupling problem is written for both mechanical and diffusion parts which will be discussed separately in the next subsections.

3.1 Diffusion behavior

As discussed in section 2, the Fick's diffusion equation is used to describe the diffusion of the water inside the composite material. For the sake of simplicity, the 1D form of the diffusion equation is considered and the generalization to the 3D case will be done eventually. Multiplying both sides of the 1D Fick's equation (characterized by a single diffusion constant D) by a kinematically admissible scalar w^* yields:

$$\int_\Omega \frac{\partial c(\mathbf{x},t)}{\partial t} w^* d\Omega = -D \int_\Omega (\Delta c(\mathbf{x},t)) w^* d\Omega \tag{9}$$

Simplifying the right hand side requires to use the following equation:

$$\psi(\mathbf{x})\mathrm{div}(\Psi(\mathbf{x})) = \mathrm{div}(\psi(\mathbf{x})\Psi(\mathbf{x})) - \Psi(\mathbf{x})^\top \mathrm{grad}\ \psi(\mathbf{x}) \tag{10}$$

Hence

$$\begin{aligned}(\Delta c(\mathbf{x},t)) w^* &= \mathrm{div}(\mathrm{grad\ c}(\mathbf{x},\mathrm{t})\mathrm{w}^*) \\ &= \mathrm{div}(\mathrm{grad\ c}(\mathbf{x},\mathrm{t})\mathrm{w}^*) - (\mathrm{grad\ c}(\mathbf{x},\mathrm{t}))^\top \mathrm{grad\ w}^*\end{aligned} \tag{11}$$

The spatial discretization of the moisture content in terms of the finite element shape functions Φ_j, $j = 1, ..., N_{\mathrm{nodes}}$ reads:

$$c(\mathbf{x},t) = \Sigma_{j=1}^{N_{\mathrm{nodes}}} \Phi_j(\mathbf{x}) c_j(t) = [\mathbf{N_F}(\mathbf{x})]\{c(t)\} \tag{12}$$

in which the column vector $\{c(t)\}$ is the nodal values of the moisture content over a particular element whereas the matrix $[\mathbf{N_F}(\mathbf{x})]$ contains the finite element shape functions. Henceforth, the diffusion and mechanical behaviors are distinguished via $\mathbf{F}$ and $\mathbf{L}$ subscripts respectively. The gradient of the field $c(\mathbf{x},t)$ is also related to the corresponding nodal values via $\mathrm{grad\ c}(\mathbf{x},\mathrm{t}) = [\mathbf{B_F}(\mathbf{x})]\{\mathrm{c}(\mathrm{t})\}$ in which $[\mathbf{B_F}(\mathbf{x})]$ contains the spatial derivatives of the shape functions. The right hand side of the equation (9) could thus be written as:

$$\begin{aligned}&-D\left[\int_\Omega \mathrm{div}(\mathrm{w}^*\mathrm{grad\ c}(\mathbf{x},\mathrm{t}))\mathrm{d}\Omega - \int_\Omega (\mathrm{grad\ c})^\top \mathrm{grad\ w}^* \mathrm{d}\Omega\right] \\ &= -D\left[\int_{\partial\Omega} (w^*\mathrm{grad\ c}(\mathbf{x},\mathrm{t})).\hat{\mathbf{n}}\mathrm{dS} - \int_\Omega (\mathrm{grad\ c})^\top \mathrm{grad\ w}^* \mathrm{d}\Omega\right]\end{aligned} \tag{13}$$

in which $\partial\Omega$ and $\hat{\mathbf{n}}$ represent the boundary of the medium and the outward normal unit vector, respectively. In the previous equation, the Green-Ostrogradsky's equation is used to relate the integral over the volume to the integral on its boundaries which vanishes:

$$\int_\Omega \mathrm{div}(\mathrm{w}^*\mathrm{grad\ c}(\mathbf{x},\mathrm{t}))\mathrm{d}\Omega = \int_{\partial\Omega} (\mathrm{w}^*\mathrm{grad\ c}(\mathbf{x},\mathrm{t})).\hat{\mathbf{n}}\mathrm{dS} = 0 \tag{14}$$

We thus get:

$$\begin{aligned}-D\left[\int_\Omega \mathrm{div}(\mathrm{w}^*\mathrm{grad\ c}(\mathbf{x},\mathrm{t}))\mathrm{d}\Omega - \int_\Omega (\mathrm{grad\ c})^\top \mathrm{grad\ w}^* \mathrm{d}\Omega\right] \\ = D\int_\Omega (\mathrm{grad\ c})^\top \mathrm{grad\ w}^* \mathrm{d}\Omega\end{aligned} \tag{15}$$

Using the matrix forms, we can rewrite this equation as:

$$\begin{aligned}&D\int_\Omega \left([\mathbf{B_F}(\mathbf{x})]\{w^*(t)\}\right)^\top \left([\mathbf{B_F}(\mathbf{x})]\{c(t)\}\right) \\ &= D\int_\Omega \{w^*(t)\}^\top [\mathbf{B_F}(\mathbf{x})]^\top [\mathbf{B_F}(\mathbf{x})]\{c(t)\} d\Omega \\ &= \{w^*(t)\}^\top \left[\int_\Omega [\mathbf{B_F}(\mathbf{x})]^\top D [\mathbf{B_F}(\mathbf{x})]\right]\{c(t)\} \\ &= \{w^*(t)\}^\top [\mathbf{K_F}]\{c(t)\}\end{aligned} \tag{16}$$

wherein the $N_{\mathrm{nodes}} \times N_{\mathrm{nodes}}$ matrix $[\mathbf{K_F}]$ could be considered as the contribution of the diffusion to the total stiffness matrix of the system. The generalization to the 3D case could be done by replacing the scalar D with a diagonal matrix as $\mathbf{D} = \mathrm{diag}(\mathrm{D_x}, \mathrm{D_y}, \mathrm{D_z})$. Similarly, the left hand side of the equation (9) could be simplified using the equation (10):

$$\begin{aligned}\int_\Omega \frac{\partial c(\mathbf{x},t)}{\partial t} w^* d\Omega &= \int_\Omega {c^*}^\top \frac{\partial c(\mathbf{x},t)}{\partial t} d\Omega \\ &= \int_\Omega \{w^*(t)\}^\top [\mathbf{N_F}(\mathbf{x})]^\top [\mathbf{N_F}(\mathbf{x})]\{\dot{c}(t)\} \\ &= \{w^*(t)\}^\top \left[\int_\Omega [\mathbf{N_F}(\mathbf{x})]^\top [\mathbf{N_F}(\mathbf{x})]\right]\{\dot{c}(t)\}\end{aligned} \tag{17}$$

in which the dot over c represents the time derivative. We use a finite difference scheme to calculate the time derivative of c, i.e. $\{\dot{c}(t)\} = \frac{\{dc(t)\}}{\Delta t} = \frac{\{c(t+\Delta t) - c(t)\}}{\Delta t}$ where Δt is the time step. Equating the left and right hand sides yields:

$$\begin{aligned}\{w^*(t)\}^\top \left[\frac{1}{\Delta t}\int_\Omega [\mathbf{N_F}(\mathbf{x})]^\top [\mathbf{N_F}(\mathbf{x})] d\Omega\right]\{dc(t)\} \\ = \{w^*(t)\}^\top \left[\int_\Omega [\mathbf{B_F}(\mathbf{x})]^\top \mathbf{D} [\mathbf{B_F}(\mathbf{x})] d\Omega\right]\{c(t)\} \\ = \{w^*(t)\}^\top \left[\int_\Omega [\mathbf{B_F}(\mathbf{x})]^\top \mathbf{D} [\mathbf{B_F}(\mathbf{x})] d\Omega\right] \\ (\{c(t+\Delta t)\} - \{dc(t)\})\end{aligned} \tag{18}$$

If we define the $N_{\mathrm{nodes}} \times N_{\mathrm{nodes}}$ matrix $[\mathbf{M_F}] = \left[\frac{1}{\Delta t}\int_\Omega [\mathbf{N_F}(\mathbf{x})]^\top [\mathbf{N_F}(\mathbf{x})]\right]$ being similar to a mass matrix,

we get:

$$[\mathbf{M_F} + \mathbf{K_F}]\{dc(t)\} = [\mathbf{K_F}]\{c(t + \Delta t)\} \quad (19)$$

which is the discretized form of the diffusion contribution to the total stiffness.

3.2 Mechanical behavior

Similar to the previous case, multiplying both sides of the constitutive equation by the kinematically admissible vector $\mathbf{u}^*$ yields:

$$\int_\Omega \mathrm{div}\left[\mathrm{C}(\bar{\mathrm{c}}(\mathrm{t}))\left(\varepsilon(\mathbf{x},\mathrm{t}) - \varepsilon^{\mathrm{h}}(\mathbf{x},\mathrm{t})\right)\right].\mathbf{u}^* \mathrm{d}\Omega \quad (20)$$

using the equation (10), we get:

$$\begin{aligned}\mathrm{div}&\left[\mathrm{C}(\bar{\mathrm{c}}(\mathrm{t}))\left(\varepsilon(\mathbf{x},\mathrm{t}) - \varepsilon^{\mathrm{h}}(\mathbf{x},\mathrm{t})\right)\right].\mathbf{u}^* \\ &= \mathrm{div}\left[\left(\mathrm{C}(\bar{\mathrm{c}}(\mathrm{t}))\left(\varepsilon(\mathbf{x},\mathrm{t}) - \varepsilon^{\mathrm{h}}(\mathbf{x},\mathrm{t})\right)\right)\mathbf{u}^*\right] \\ &\quad - \left[C(\bar{c}(t))\left(\varepsilon(\mathbf{x},t) - \varepsilon^h(\mathbf{x},t)\right)\right].\mathrm{grad}\ \mathbf{u}^* \end{aligned} \quad (21)$$

The displacement field is discretized as:

$$\mathbf{u}(\mathbf{x},t) = \Sigma_{j=1}^{N_{\mathrm{nodes}}}\Phi_j(\mathbf{x})u_j(t) = [\mathbf{N_L}(\mathbf{x})]\{u(t)\} \quad (22)$$

in which $\{u(t)\}$ is the column vector of the nodal displacements over a particular element. The strain ε is related to the nodal displacement vector via $\varepsilon(\mathbf{x},t) = \frac{\mathrm{grad}\ \mathbf{u} + (\mathrm{grad}\ \mathbf{u})^\top}{2} = [\mathbf{B_L}(\mathbf{x})]\{u(t)\}$ in which $[\mathbf{B_L}(\mathbf{x})]$ is the so-called strain-displacement matrix. Introducing (21) into (20) yields:

$$\begin{aligned}&\int_\Omega \mathrm{div}\left[\left(\mathrm{C}(\bar{\mathrm{c}}(\mathrm{t}))\left(\varepsilon(\mathbf{x},\mathrm{t}) - \varepsilon^{\mathrm{h}}(\mathbf{x},\mathrm{t})\right)\right)\mathbf{u}^*\right]\mathrm{d}\Omega \\ &- \int_\Omega \left[C(\bar{c}(t))\left(\varepsilon(\mathbf{x},t) - \varepsilon^h(\mathbf{x},t)\right)\right]^\top.\mathrm{grad}\ \mathbf{u}^*\mathrm{d}\Omega = 0\end{aligned} \quad (23)$$

Using the Green-Ostrogradsky's theorem we get:

$$\begin{aligned}&\int_\Omega \mathrm{div}\left[\left(\mathrm{C}(\bar{\mathrm{c}}(\mathrm{t}))\left(\varepsilon(\mathbf{x},\mathrm{t}) - \varepsilon^{\mathrm{h}}(\mathbf{x},\mathrm{t})\right)\right)\mathbf{u}^*\right]\mathrm{d}\Omega \\ &= \int_{\partial\Omega}\left[\left(C(\bar{c}(t))\left(\varepsilon(\mathbf{x},t) - \varepsilon^h(\mathbf{x},t)\right)\right)\mathbf{u}^*\right].\hat{\mathbf{n}}dS = 0\end{aligned} \quad (24)$$

Hence:

$$\begin{aligned}&\int_\Omega \mathrm{div}\left[\mathrm{C}(\bar{\mathrm{c}}(\mathrm{t}))\left(\varepsilon(\mathbf{x},\mathrm{t}) - \varepsilon^{\mathrm{h}}(\mathbf{x},\mathrm{t})\right)\right].\mathbf{u}^*\mathrm{d}\Omega \\ &= -\int_\Omega \left[C(\bar{c}(t))\left(\varepsilon(\mathbf{x},t) - \varepsilon^h(\mathbf{x},t)\right)\right]^\top.\mathrm{grad}\ \mathbf{u}^*\mathrm{d}\Omega\end{aligned} \quad (25)$$

or:

$$\begin{aligned}&\int_\Omega [C(\bar{c}(t))\varepsilon(\mathbf{x},t)].\mathrm{grad}\ \mathbf{u}^*\mathrm{d}\Omega \\ &\qquad = \int_\Omega \left[C(\bar{c}(t))\varepsilon^h(\mathbf{x},t)\right]^\top.\mathrm{grad}\ \mathbf{u}^*\mathrm{d}\Omega\end{aligned} \quad (26)$$

which could be transformed to the following form:

$$\begin{aligned}&\int_\Omega [C(\bar{c}(t))\varepsilon(\mathbf{x},t)].\mathrm{grad}\ \frac{\mathbf{u}^* + \mathbf{u}^{*^\top}}{2}\mathrm{d}\Omega \\ &\qquad = \int_\Omega \left[C(\bar{c}(t))\varepsilon^h(\mathbf{x},t)\right]^\top.\mathrm{grad}\ \frac{\mathbf{u}^* + \mathbf{u}^{*^\top}}{2}\mathrm{d}\Omega\end{aligned} \quad (27)$$

Since the terms $\varepsilon(\mathbf{x},t) = \frac{\mathbf{u}+\mathbf{u}^\top}{2}$ and $\frac{\mathbf{u}^*+\mathbf{u}^{*^\top}}{2}$ could be written in a matrix form as $[\mathbf{B_L}(\mathbf{x})]\{u(t)\}$ and $[\mathbf{B_L}(\mathbf{x})]\{u^*(t)\}$, the previous equation could be rewritten as:

$$\begin{aligned}&\int_\Omega [C(\bar{c}(t))[\mathbf{B_L}(\mathbf{x})]\{u(t)\}].([\mathbf{B_L}(\mathbf{x})]\{u^*(t)\})d\Omega \\ &\qquad = \int_\Omega \left[C(\bar{c}(t))\varepsilon^h(\mathbf{x},t)\right].([\mathbf{B_L}(\mathbf{x})]\{u^*(t)\})d\Omega\end{aligned} \quad (28)$$

Hence:

$$\begin{aligned}&\int_\Omega ([\mathbf{B_L}(\mathbf{x})]\{u^*(t)\})^\top [C(\bar{c}(t))[\mathbf{B_L}(\mathbf{x})]\{u(t)\}]\, d\Omega \\ &\qquad = \int_\Omega ([\mathbf{B_L}(\mathbf{x})]\{u^*(t)\})^\top \left[C(\bar{c}(t))\varepsilon^h(\mathbf{x},t)\right] d\Omega\end{aligned} \quad (29)$$

or:

$$\begin{aligned}&\{u^*(t)\}^\top \left[\int_\Omega ([\mathbf{B_L}(\mathbf{x})]^\top C(\bar{c}(t))[\mathbf{B_L}(\mathbf{x})]d\Omega\right]\{u(t)\} \\ &\qquad = \{u^*(t)\}^\top \left[\int_\Omega [\mathbf{B_L}(\mathbf{x})]^\top C(\bar{c}(t))\varepsilon^h(\mathbf{x},t)d\Omega\right]\end{aligned} \quad (30)$$

that gives:

$$\begin{aligned}&\left[\int_\Omega ([\mathbf{B_L}(\mathbf{x})]^\top C(\bar{c}(t))[\mathbf{B_L}(\mathbf{x})]d\Omega\right]\{u(t)\} \\ &\qquad = \left[\int_\Omega [\mathbf{B_L}(\mathbf{x})]^\top C(\bar{c}(t))\varepsilon^h(\mathbf{x},t)d\Omega\right]\end{aligned} \quad (31)$$

Let us define the matrix $[\mathbf{K_L}] = \left[\int_\Omega ([\mathbf{B_L}(\mathbf{x})]^\top C(\bar{c}(t))[\mathbf{B_L}(\mathbf{x})]d\Omega\right]$ which represents the contribution of the mechanical behavior on the total stiffness matrix of the system. Writing $\{u(t)\} = \{u(t + \Delta t)\} - \{du(t)\}$ yields the following equation:

$$\begin{aligned}[\mathbf{K_L}]\{du(t)\} &= [\mathbf{K_L}]\{u(t + \Delta t)\} \\ &\quad - \left[\int_\Omega [\mathbf{B_L}(\mathbf{x})]^\top \sigma^h(\mathbf{x},t)d\Omega\right]\end{aligned} \quad (32)$$

where $\sigma^h(\mathbf{x},t) = C(\bar{c}(t))\varepsilon^h(\mathbf{x},t)$ corresponds to the stress generated by the water diffusion throughout the medium.

3.3 Hygro-mechanical coupling

The combinations of equations (19) and (32) provides the following system of equations which describes the hygro-mechanical behavior of the composite material taking into account the degradation of the elasticity matrix:

$$\begin{bmatrix} [\mathbf{K_L}] & [\mathbf{0}] \\ [\mathbf{0}] & [\mathbf{M_F}] + [\mathbf{K_F}] \end{bmatrix} \begin{bmatrix} \{du(t)\} \\ \{dc(t)\} \end{bmatrix} = \begin{bmatrix} \left[\int_\Omega [\mathbf{B_L}(\mathbf{x})]^\top \sigma^h(\mathbf{x},t) d\Omega\right] \\ [\mathbf{0}] \end{bmatrix} + \begin{bmatrix} [\mathbf{K_L}] & [\mathbf{0}] \\ [\mathbf{0}] & [\mathbf{K_F}] \end{bmatrix} \begin{bmatrix} \{u(t+\Delta t)\} \\ \{c(t+\Delta t)\} \end{bmatrix} \tag{33}$$

This equation has the same form as the general desired form $[\mathbf{K}]\{du\} = \{f\}$. Consequently, the total stiffness matrix writes:

$$[\mathbf{K}] = \begin{bmatrix} [\mathbf{K_L}] & [\mathbf{0}] \\ [\mathbf{0}] & [\mathbf{M_F}] + [\mathbf{K_F}] \end{bmatrix} \tag{34}$$

The matrix system (33) will be solved in the numerical code (Abaqus® UEL) developed in this work in order to obtain the displacement and moisture content fields. In the next section some numerical simulations are introduced to show the robustness of our numerical approach.

4 Numerical example

The numerical results that will be presented in this section are obtained using two different configurations: a cube subjected to a tension load following x direction and a shear load in xy plane. Displacements of 0.2 mm and 0.02 mm are applied to the cube during a simulation time of 84 days, respectively for traction and shear cases. The results are discussed in subsections 4.1 and 4.2.

4.1 Preliminary results: Numerical verifications

In this subsection the capacity of the implemented model is presented. Therefore, this study enables to check whether the model appropriately satisfies the theoretical and finite element formulations elaborated earlier in sections 2 and 3.

A composite material submitted to a tensile load along the direction of the fibers is considered. The medium is a cube Ω of size 2 mm $\times$ 2 mm $\times$ 2 mm whose dimensions are chosen only for illustrative purposes. The results are obtained using 4-node tetrahedron finite elements of size 0.2 mm that has been chosen after carrying out a numerical mesh convergence study. The total number of elements is 8199. The material is immersed with a particular moisture content c_∞ ($c_\infty = 1$) applied on all its boundaries $\partial\Omega$.

4.1.1 Evolution of elastic moduli

The evolution of the elastic moduli depends on the initial and final states of saturation of the medium.

At first, the numerical results are presented using the experimental data in Tual et al. (2015). These data are summarized in Table 1 in which only the shear modulus changes in terms of the moisture content and the other parameters are constant.

During the simulation, the evolution of the coefficients E_{11} and G_{12} are recorded and illustrated in Figure 6.

Secondly, the numerical simulations are performed over the same medium considering different degradation levels (from 0 to 50 percent) in order to better illustrate the dependence of the mechanical properties on the diffusion state of the medium. Figure 7 shows the variation of the coefficients C_{11} and C_{44} in terms of the moisture content for 0 %, 5 %, 10 %, 20 % and 50 % fall down of the material properties with respect to the initial dry state.

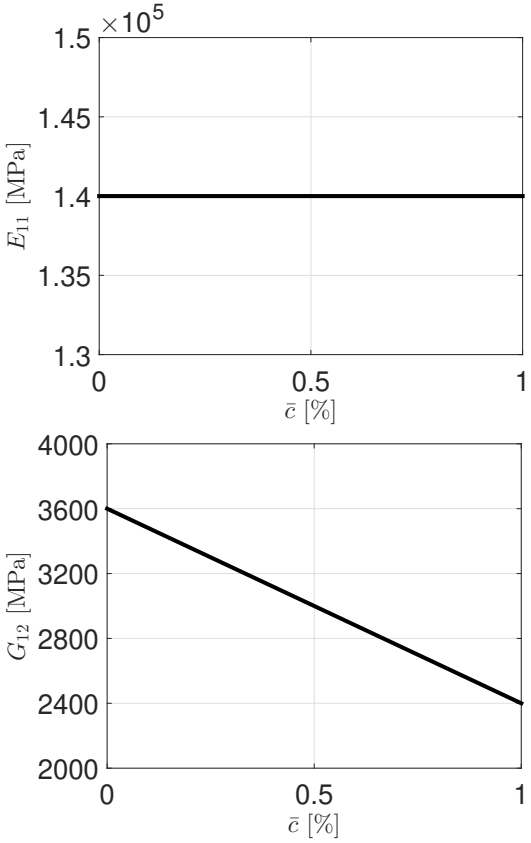

Figure 6. Evolution of E_{11} (top) and G_{12} (bottom) as a function of the average moisture content of the medium $\bar{c}(t)$.

Figure 8 also displays the corresponding stress-strain curves. Since the degradation progressively takes place

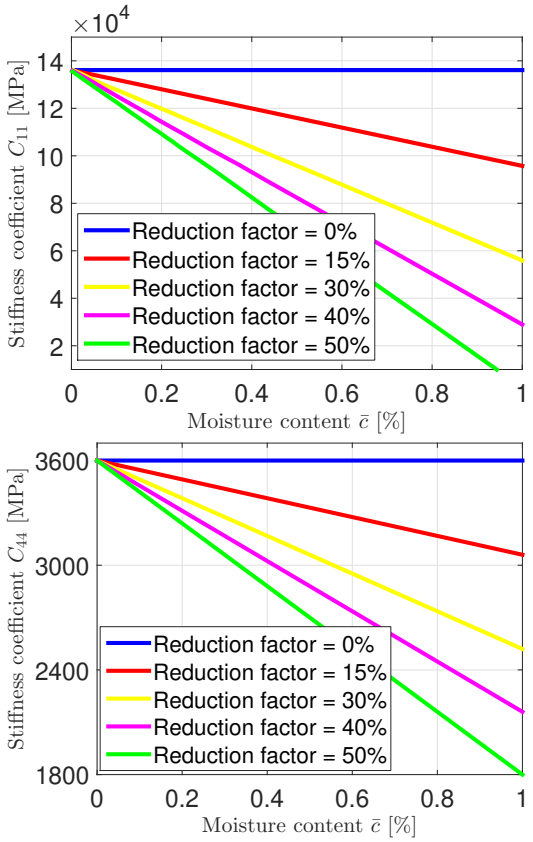

Figure 7. Evolution of C_{11} (top) and C_{44} (bottom) as a function of the average moisture content of the medium $\bar{c}(t)$.

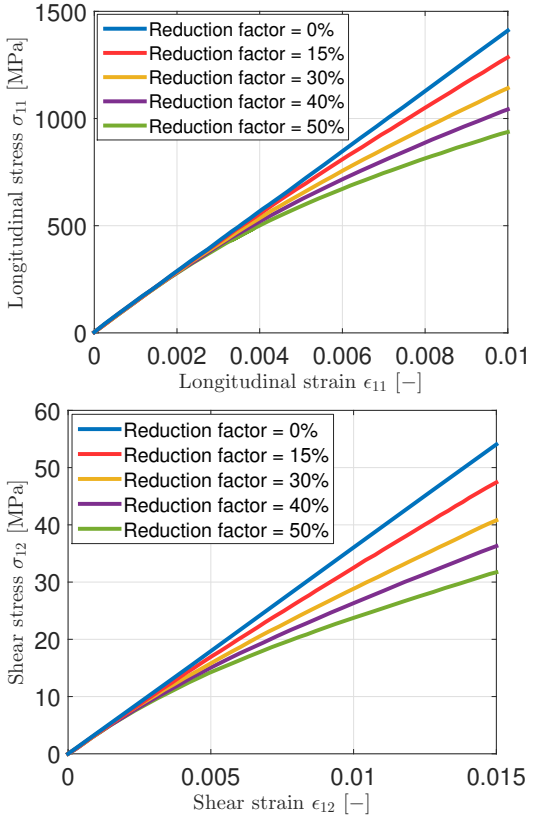

Figure 8. Longitudinal and transverse stresses with respect to the strain.

during the water diffusion throughout the medium, the material behavior is piecewise linear. This will results in a non-linear evolution of the stress in terms of the strain. Obviously, once the saturation is reached, the curves remain linear.

4.1.2 Evolution of the strengths Similar to the case of elastic moduli presented in the previous subsection, the strengths values used in this work are taken from Tual et al. (2015). Table 2 summarizes the corresponding values in dry and saturated states.

Figure 9 illustrates the linear evolution of the strengths X_r, Y_r and S_r in terms of the average moisture content $\bar{c}(t)$. These evolutions have indeed an impact on the values of the failure criterion and will be further discussed in the next subsection.

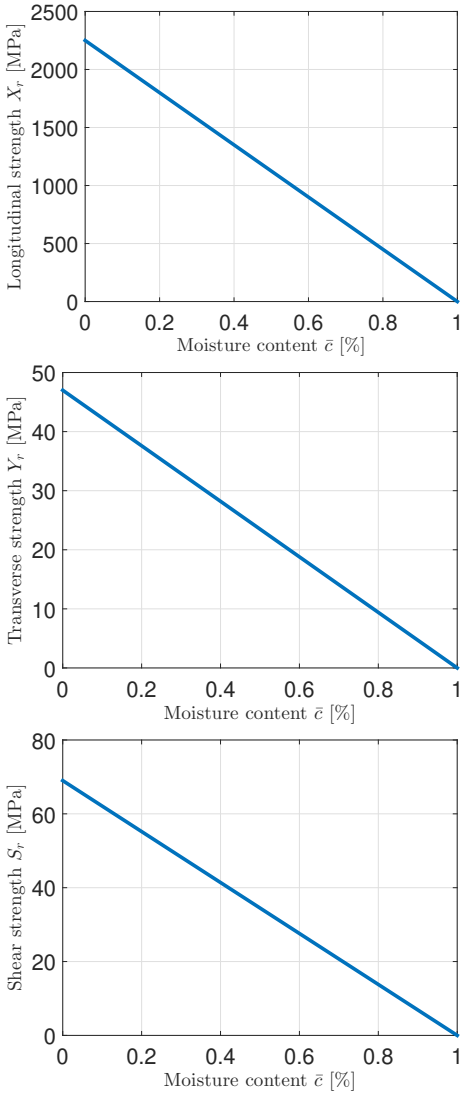

Figure 9. Evolution of the material strengths X_r (a), Y_r (b) and S_r (c) as a function of the average moisture content.

4.1.3 Application of an implemented failure criterion: Tsaï-Hill criterion In order to analyze the failure of the medium, the Tsaï-Hill criterion is evaluated after each time step by taking into consideration the modified values of the strengths as a function of the average moisture content.

Figures 10 and 11 respectively show the distribution of the stain and stress fields in the cube for both tension (top) and shear (bottom) cases. Figure 12 shows the value of the Tsaï-Hill criterion within the medium Ω for the case of a tensile loading along the fiber direction (top) along with the case of a shear loading (bottom).

The evolution of the strengths in terms of the water content yields a varying failure criterion according to the aging level of the specimen. Thus, since the regions near the borders absorb the water first, the failure criterion is reached faster compared to the core part of the specimen. For the case studies illustrated by figures 7 and 8 and following the evolution of the strengths according to table 2), we can see that the failure criterion is reached first for 0 % reduction factor and then for 5%, 10 %, 20 % and 50 %, respectively.

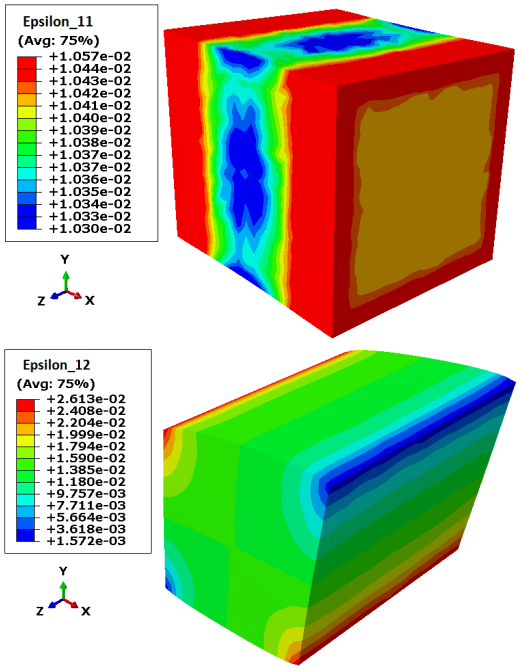

Figure 10. Distribution of the longitudinal and shear strain fields respectively for traction (top) and shear (bottom) case study.

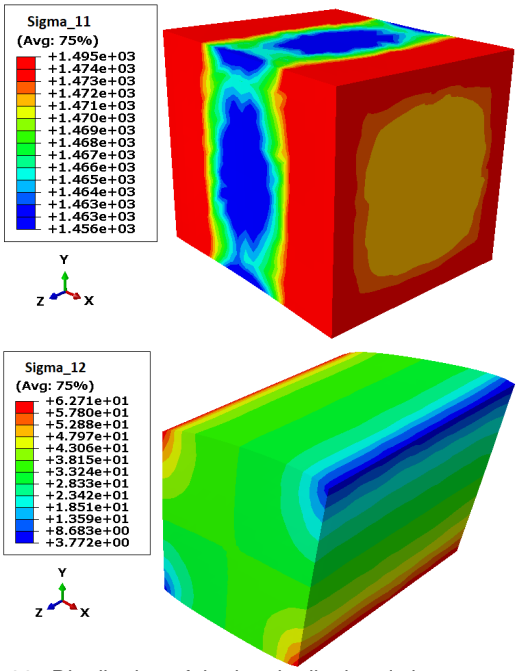

Figure 11. Distribution of the longitudinal and shear stress fields respectively for traction (top) and shear (bottom) case study.

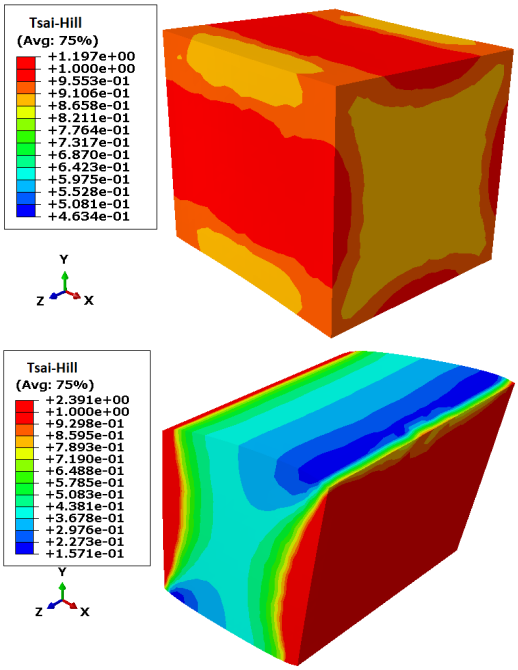

Figure 12. Evaluation of the Tsaï-Hill criterion respectively for traction (top) and shear (bottom)

4.2 *Validation with Abaqus®*

In order to validate the implemented UEL code, the results of the simulations carried out with the developed tetrahedral and hexahedral elements are compared with their counterparts obtained according to simulations that have been performed respectively with the element types C3D4T and C3D8T of Abaqus®. As it is impossible to account for the degradation of material properties using the classical elements and the constitutive laws available in the software Abaqus®, the simulations are run with the developed user elements (subroutines UEL) with constant mechanical properties: this is equivalent to perform a hygroelastic simulation where the mechanical behavior and the diffusion kinetics are uncoupled. For this purpose, the same cube as described in the previous section is considered. Thus, the distribution of the stress and strain fields in the medium is identical for Abaqus® and the developed user elements (UELs). Then, the evolution of the stress as a function of the strain and that of the moisure content over time are plotted. Figure 13 (a) and Figure 13 (b) respectively show the stress-strain and the water sorption curves. Furthermore, the difference between the results is almost negligible, which means that the implemented UEL routine yields results that

are consistent with those obtained by the native Abaqus® software. Note also that the calculation time with the implemented subroutine (i.e. 1096s on a CPU) remains large compared to that using Abaqus C3D4T elements (i.e. 263s on a CPU). An algorithm optimization is thus needed to reduce the computation time especially for larger scale domains.

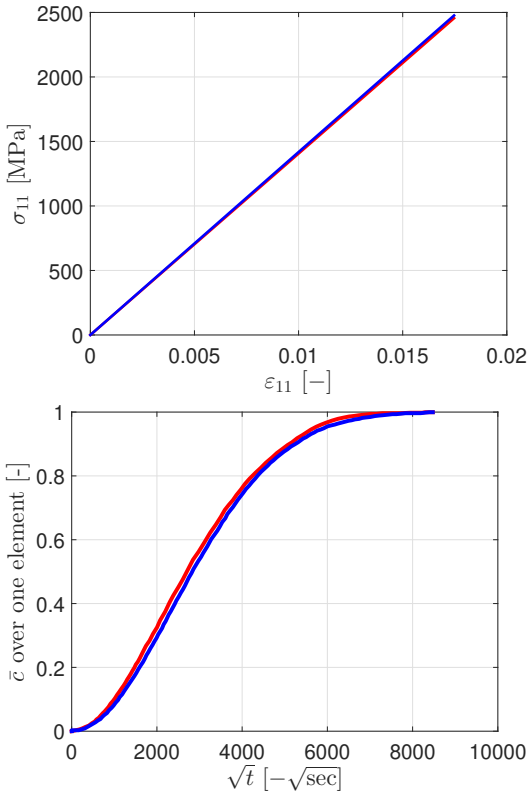

Figure 13. Comparision with Abaqus results: (a) Evolution of the stress σ_{11} as a function of the strain ϵ_{11} and (b) Evolution of the moisture content as a function of the time. The blue and red curves correspond to the results obtained from the UEL and Abaqus, respectively.

4.3 Comparison with other approximation types

In previous sections we introduced a linear evolution model for the elastic coefficients and the ultimate strengths. This linear model is practical for industrial purposes since only two specimens should be tested to obtain its parameters. In this section, we utilize a nonlinear evolution model for both elastic matrix components and the ultimate strengths. This model is based on a quadratic approximation $G_{12}(\bar{c}) = -763.59\bar{c}^2 - 430\bar{c} + 3610$. It would be interesting to verify this result for materials whose aging corresponds to higher drops in mechanical properties. This could be the case for thermoplastic matrix composites Mbacké and Rozycki (2018); Rozycki et al. (2018); Obeid et al. (2018); Pivdiablyk et al. (2020).

Figure 14 shows the evolution of shear stress σ_{12} as a function of shear strain ε_{12} for three approximation functions

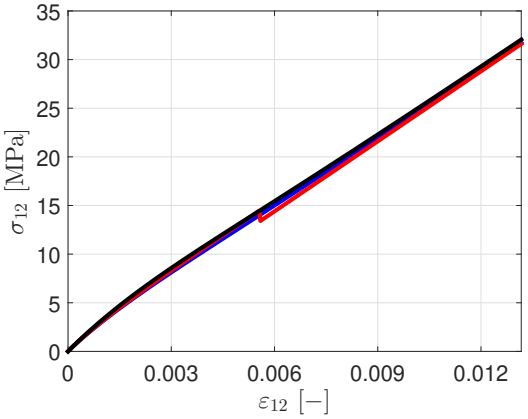

Figure 14. Comparision linear, bilinear and polynomial models: Evolution of the stress σ_{12} as a function of the strain ϵ_{12} . Blue, red and black curves correspond to linear, bilinear and nonlinear cases, respectively.

(linear, bilinear and polynomial). An almost negligible difference between the three curves is observed. Indeed, we do not have enough experimental points to make a better approximation (only four points), but we can deduce that a linear approximation of the evolution of the mechanical properties (shear modulus) is sufficient in addition to allowing more input data to be obtained for the coupled model.

5 Conclusions

This paper is focused on the development of a numerical model for simulating the hygro-mechanical behavior of composite materials. Indeed, experimental works have revealed that the mechanical properties of organic composites can change as a function of moisture uptake Mercier et al. (2008); Aldajah et al. (2009); Tual et al. (2015); Li et al. (2016). Thus, the appropriate modeling of the behavior of immersed composite materials requires to take into account the coupling between the mechanical and diffusion behaviors. Following a state of the art on existing coupling approaches (free volume theory Peret et al. (2014); Youssef et al. (2009a) and thermodynamics of irreversible processes Rambert and Grandidier (2005); B. E. Sar and Jacquemin (2012), the present work proposes a pragmatic and adapted approach to model the coupled hygro-mechanical behavior of composite materials immersed in water accounting for an evolution of structure's stiffness matrix and mechanical strength according to the average moisture content and thus the immersion time. Based on the experimental results obtained in Tual et al. (2015), we tested different approximations: linear, bilinear and polynomial. Since the linear model results in low discrepancies compared to other models, the former could be appropriately used to describe the coupling problem. The advantage of this linear model is that it only requires

the mechanical properties at dry and saturated states. For this purpose, an Abaqus user defined element (UEL) subroutine has been created. The accuracy of our numerical implementation has been checked through several numerical case studies by using the experimental results of Tual et al. (2015) and by varying the degradation degrees (from 0 to 50 percent) in order to better illustrate the dependence of the mechanical properties on the moisture uptake (Figure 8).

Finally, the simulations carried out with the developped tetrahedral and hexahedral user elements have been compared with those that are performed respectively with the element types C3D4T and C3D8T of Abaqus. It was found that the difference between the results is almost negligible, which means that our UEL routine yields results that are consistent with those obtained by Abaqus. The model is built using composites with hydrophobic fibers such as carbon fibers. It could be straightforwardly extended to other types of fibers provided that the evolution of the mechanical properties follows a linear or polynomial shape. It should be noted that the dependence of the diffusion coefficients on the mechanical loading could also be incorporated into our numerical model provided that the experimental studies reveal this coupling.

Acknowledgements

Authors gratefully acknowledge all partners of the VICOMTE project: IRT Jules Verne, Meca, Université de Nantes, General Electric and Bureau Veritas.

References

Adamson M (1980) Thermal expansion and swelling of cured epoxy resin used in graphite/epoxy composite materials. Journal of Materials Science 15: 1736–1745.

Ahmad M, Majid MA, Ridzuan M, Mazlee M and Gibson A (2018) Dynamic mechanical analysis and effects of moisture on mechanical properties of interwoven hemp/polyethylene terephthalate (pet) hybrid composites. Construction and Building Materials 179: 265–276.

Aldajah S, Alawsi G and Rahmaan SA (2009) Impact of sea and tap water exposure on the durability of gfrp laminates. Materials & Design 30(5): 1835–1840.

B E Sar PD S Fréour and Jacquemin J (2012) Coupling moisture diffusion and internal mechanical states in polymers e a thermodynamical approach. European Journal of Mechanics A/Solids 36: 38–43.

Bonniau P and Bunsell AR (1981) Water absorption by glass fibre reinforced epoxy resin. Composite Structures : 92–105.

Carter H and Kibler K (1978) Langmuir-type model for anomalous moisture diffusion in composite resins. Journal of Composite Materials 12: 118–131.

Castaing P and Lemoine L (1995) Effects of water absorption and osmotic degradation on long term behavior of glass fibre reinforced polyester. Polymer Composites, 16: 349–356.

Chester SA and Anand L (2011) A thermo-mechanically coupled theory for fluid permeation in elastomeric materials: application to thermally responsive gels. Journal of the Mechanics and Physics of Solids 59(10): 1978–2006.

Chester SA, Di Leo CV and Anand L (2015) A finite element implementation of a coupled diffusion-deformation theory for elastomeric gels. International Journal of Solids and Structures 52: 1–18.

Chouhan H, Asija N, Ahmed A, Bhatnagar N et al. (2019) Effect of moisture on high strain rate performance of uhmwpe fiber based composite. Procedia Structural Integrity 14: 830–838.

Clément A, Fréour S and Jacquemin F (2018) Multiphysics modeling of the hygro-mechanical behavior of heterogeneous materials. In: Durability of Composites in a Marine Environment 2. Springer, pp. 91–112.

Crank J (1979) The mathematics of diffusion. Oxford university press.

Dana HR, Perronnet A, Fréour S, Casari P and Jacquemin F (2013) Identification of moisture diffusion parameters in organic matrix composites. Journal of composite materials 47(9): 1081–1092.

Derrien K and Gilormini P (2009) The effect of moisture-induced swelling on the absorption capacity of transversely isotropic elastic polymer–matrix composites. International Journal of Solids and Structures 46(6): 1547–1553.

Dewimille B and Bunsell A (1983) Accelerated ageing of a glass fibre-reinforced epoxy resin in water. Composites 14(1): 35–40.

E L McKague Jr JDR and Halkias JE (1978) Swelling and glass transition relations for epoxy matrix material in humid environments. Journal of Applied Polymer Science 22: 1643–1654.

Fahmy AA and Hurt JC (1980) Stress dependence of water diffusion in epoxy resin. Polymer Composites 1: 77–8.

Fick A (1855) Ueber diffusion. Annalen der Physik 170: 59–86.

Figliolini AM and Carlsson LA (2014) Mechanical properties of carbon fiber/vinylester composites exposed to marine environments. Polymer Composites 35(8): 1559–1569.

Gager V, Le Duigou A, Bourmaud A, Pierre F, Behlouli K and Baley C (2019) Understanding the effect of moisture variation on the hygromechanical properties of porosity-controlled nonwoven biocomposites. Polymer Testing 78: 105944.

Hashin Z (1980) Failure criteria for unidirectional fiber composites. Journal of applied mechanics 47(2): 329–334.

Hassani MM, Wittel FK, Hering S and Herrmann HJ (2015) Rheological model for wood. Computer Methods in Applied Mechanics and Engineering 283: 1032–1060.

I Ghorbel MCY D Valentin and Spiteri P (1990) The effect of resin flexibility on the creep behaviour of filament-wound glass-reinforced resin pipes. Developments in the Science and Technology of Composite Materials : 213–220.

Jacquemin F and Fréour S (2014) Water–mechanical property coupling. In: Durability of Composites in a Marine Environment. Springer, pp. 115–128.

Langmuir I (1916) The constitution and fundamental properties of solids and liquids. part i. solids. Journal of the American Chemical Society 38: 2221–2295.

Li W, Xu C and Cho Y (2016) Characterization of degradation progressive in composite laminates subjected to thermal fatigue and moisture diffusion by lamb waves. Sensors 16(2): 260.

Mbacké MA and Rozycki P (2018) Non-linear constitutive law for a glass-pa66 fabric composite dedicated to numerical simulations in crash studies. In: ECCM18-18th European Conference on Composite Materials.

Mei J, Tan P, Liu J, He Z and Huang W (2019) Moisture absorption characteristics and mechanical degradation of composite lattice truss core sandwich panel in a hygrothermal environment. Composites Part A: Applied Science and Manufacturing 127: 105647.

Mercier J, Bunsell A, Castaing P and Renard J (2008) Characterisation and modelling of aging of composites. Composites Part A: Applied Science and Manufacturing 39(2): 428–438.

Moleiro F, Carrera E, Ferreira A and Reddy J (2020) Hygro-thermo-mechanical modelling and analysis of multilayered plates with embedded functionally graded material layers. Composite Structures 233: 111442.

Moleiro F, Carrera E, Li G, Cinefra M and Reddy J (2019) Hygro-thermo-mechanical modelling of multilayered plates: Hybrid composite laminates, fibre metal laminates and sandwich plates. Composites Part B: Engineering 177: 107388.

Obeid H, Clément A, Fréour S, Jacquemin F and Casari P (2018) On the identification of the coefficient of moisture expansion of polyamide-6: Accounting differential swelling strains and plasticization. Mechanics of Materials 118: 1–10.

Peret T, Clément A, Fréour S and Jacquemin F (2014) Numerical transient hygro-elastic analyses of reinforced fickian and non-fickian polymers. Composite Structures 116: 395–403.

Pivdiablyk I, Rozycki P, Jacquemin F, Gornet L and Auger S (2020) Experimental analysis of the mechanical performance of glass fibre reinforced 6 under varying environmental conditions. Composite Structures : 112338.

Puck A (1969) Calculating the strength of glass fibre/plastic laminates under combined load. Kunststoffe 55: 18–19.

Rambert G and Grandidier JC (2005) An approach to the coupled behaviour of polymers subjected to a thermo-mechanical loading in a gaseous environment. European Journal of Mechanics A/Solids 24: 151–168.

Roy S (2000) Hygrothermal modeling of polymers and polymer matrix composites. In: Time dependent and nonlinear effects in polymers and composites. ASTM International.

Rozycki P, Mbacke MA and Dau AT (2018) Multiscale homogenization of a glass-pa66 fabric composite behavior for crash studies. In: ECCM18-18th European Conference on Composite Materials.

Sar BE, Fréour S, Davies P and Jacquemin F (2014) Accounting for differential swelling in the multi-physics modelling of the diffusive behaviour of polymers. ZAMM-Journal of Applied Mathematics and Mechanics/Zeitschrift für Angewandte Mathematik und Mechanik 94(6): 452–460.

Shen CH and Springer GS (1976) Moisture absorption and desorption of composite materials. Journal of composite materials 10(1): 2–20.

Simar A, Gigliotti M, Grandidier J and Ammar-Khodja I (2014) Evidence of thermo-oxidation phenomena occurring during hygrothermal aging of thermosetting resins for rtm composite applications. Composites Part A: Applied Science and Manufacturing 66: 175–182.

Springer GS and Tsai SW (1967) Thermal conductivities of unidirectional materials. Journal of Composite Materials 1(2): 166–173.

Tsai SW (1965) Strength characteristics of composite materials. Technical report, Philco Corp Newport Beach CA.

Tsai SW and Wu EM (1971) A general theory of strength for anisotropic materials. Journal of composite materials 5(1): 58–80.

Tual N, Carrere N, Davies P, Bonnemains T and Lolive E (2015) Characterization of sea water ageing effects on mechanical properties of carbon/epoxy composites for tidal turbine blades. Composites Part A: Applied Science and Manufacturing 78: 380–389.

Weitsman Y (2000) Effect of fluids on polymeric composites – a review. Comprehensive composite materials 16-2: 369–401.

Yaniv G and Ishai O (1987) Coupling between stresses and moisture diffusion in polymeric adhesives. Polymer Engineering and Science 27: 731–739.

Youssef G, Fréour S and Jacquemin F (2009a) Effects of moisture-dependent properties of constituents on the hygroscopic

stresses in composite structures. Mechanics of Composite Materials 45(4): 369.

Youssef G, Fréour S and Jacquemin F (2009b) Stress-dependent moisture diffusion in composite materials. Journal of Composite Materials 43(15): 1621–1637.